ENVIRONMENTAL RESEARCH
LETTERS

ACCEPTED MANUSCRIPT • OPEN ACCESS

Combining CMIP data with a regional convection-permitting model and observations to project extreme rainfall under climate change

To cite this article before publication: Cornelia Klein *et al* 2021 *Environ. Res. Lett.* in press https://doi.org/10.1088/1748-9326/ac26f1

Combining CMIP data with a regional convection-permitting model and observations to project extreme rainfall under climate change

Cornelia Klein[1,7], Lawrence S. Jackson[2], Douglas J. Parker[2], John H. Marsham[2], Christopher M. Taylor[1,8], David P. Rowell[3], Françoise Guichard[4,*], Théo Vischel[5], Adjoua Moïse Famien[6,9], Arona Diedhiou[5,10]

[1]U.K. Centre for Ecology and Hydrology, Wallingford, UK

[2]Institute for Climate and Atmospheric Science, University of Leeds, Leeds, UK

[3]Met Office Hadley Centre, Exeter, UK

[4]CNRM, Université de Toulouse, Météo-France, CNRS, Toulouse, France

*Deceased December 2020

[5]Université Grenoble Alpes, IRD, CNRS, Grenoble-INP, IGE, Grenoble, France

[6]LOCEAN, Sorbonne Universités UPMC-CNRS-IRD-MNHN, IPSL, Paris, France

[7]Department of Atmospheric and Cryospheric Sciences, University of Innsbruck, Innsbruck, Austria

[8]National Centre for Earth Observation, Wallingford, UK

[9]Université Félix Houphouët Boigny, LAPAMF-UFR SSMT, Abidjan, Côte d'Ivoire

[10]Centre d'Excellence Africain en Changement Climatique, Biodiversité et Agriculture Durable (CCBAD), Université Félix Houphouët Boigny, Abidjan, Côte d'Ivoire

Corresponding author: Cornelia Klein, cornkle@ceh.ac.uk

Abstract

Due to associated hydrological risks, there is an urgent need to provide plausible quantified changes in future extreme rainfall rates. Convection-permitting (CP) climate simulations represent a major advance in capturing extreme rainfall and its sensitivities to atmospheric changes under global warming. However, they are computationally costly, limiting uncertainty evaluation in ensembles and covered time periods. This is in contrast to the Climate Model Intercomparison Project (CMIP) 5 and 6 ensembles, which cannot capture relevant convective processes, but provide a range of plausible projections for atmospheric drivers of rainfall change. Here, we quantify the sensitivity of extreme rainfall within West African storms to changes in atmospheric rainfall drivers, using both observations and a CP projection representing a decade under the Representative Concentration Pathway 8.5 around 2100. We illustrate how these physical relationships can then be used to reconstruct better-informed extreme rainfall changes from CMIP, including for time periods not covered by the CP model. We find reconstructed hourly extreme rainfall over the Sahel increases across all CMIP models, with a plausible range of 37-75% for 2070-2100 (mean 55%, and 18-30% for 2030-2060). This is considerably higher than the +0-60% (mean +30%) we obtain from a traditional extreme rainfall metric based on raw daily CMIP rainfall, suggesting such analyses can underestimate extreme rainfall intensification. We conclude that process-based rainfall scaling is a useful approach for creating time-evolving rainfall projections in line with CP model behaviour, reconstructing important information for medium-term decision making. This approach also better enables the communication of uncertainties in extreme rainfall projections that reflect our current state of knowledge on its response to global warming, away from the limitations of coarse-scale climate models alone.

1 Introduction

Convective rainfall dominates rainfall extremes in many regions of the world, which are set to increase with or beyond the rate of increasing water vapour in the atmosphere in a warming climate (Allen & Ingram, 2002; O'Gorman & Schneider, 2009). Vigorous convective events can pose a serious threat to human health, urban infrastructure, and food security by causing flash floods (Engel et al., 2017; Lobell & Gourdji, 2012). Yet, projected changes in extreme rainfall remain highly uncertain (IPCC Working Group 1 et al., 2013). This is in part because traditional coarse-scale global climate models with

horizontal resolutions commonly $\geq$ 100 km, such as those in the Climate Model Intercomparison Project (CMIP) ensembles, cannot explicitly capture convective processes. Instead, these models rely on convective parameterisations that tend to produce daily rainfall intensities that are too low and spread out, rendering projected changes in extreme precipitation questionable (Stephens et al., 2010; Trenberth et al., 2003). This severely limits the usefulness of climate projections in the context of local impacts of changes in extreme weather (e.g., Vischel & Lebel, 2007). Consequently, there is an urgent need for more reliable information on future trends in rainfall extremes, which can support the development of adaptation and mitigation strategies.

In this context, convection-permitting (CP) simulations, which allow convection to develop explicitly, have been found to simulate more realistic rainfall characteristics in different convective environments (Prein et al., 2015; Kendon et al., 2017). However, such simulations are computationally expensive and therefore often conducted in a one-off manner, providing a single realisation of a possible future without capturing uncertainties intrinsic to future climate projections. Ensemble projections at CP scale are only just starting to emerge e.g. with a focus on the UK (Fosser et al., 2020), or are still under planning e.g. within Coordinated Regional Climate Downscaling Experiment (CORDEX) Flagship Pilot Studies for Europe, South America, and High Mountain Asia (Coppola et al., 2020; Lavin-Gullon et al., 2021; Zhou et al., 2021).

Currently, the best way to evaluate future rainfall extremes and related risks must be an expert-informed approach that combines the advantages of information from existing parameterised and CP climate model projections, together with understanding from observations. This study brings together these different state-of-the-art climate data to derive future extreme rainfall estimates.

We focus on West Africa, where we now have a single CP realisation of future climate (Stratton et al., 2018; Senior et al., 2021), which shows a greater increase in extreme rainfall than a parameterised version of the model, with greater intensification of convective updraughts (Kendon et al., 2019; Jackson et al., 2020; Berthou, Kendon, et al., 2019; Fitzpatrick et al., 2020). This CP simulation is a major advance given the dominance of large, organised thunderstorm-clusters in this region, which produce the majority of extreme rainfall (Mathon et al., 2002). These so-called mesoscale convective systems (MCSs) however cannot be captured by CMIP models. We demonstrate an approach

for combining the individual CP projection with rainfall-driver relationships from observations and with the uncertainty range from 64 CMIP simulations, based on their future changes in atmospheric MCS drivers.

Variability and change in extreme MCS rainfall predominantly depends on total column water (TCW), low-level vertical wind shear and convective available potential energy (CAPE). Higher TCW content in a warmer atmosphere is known to intensify storm dynamics and to strongly control increases in extreme rainfall (Roderick et al., 2019; Fitzpatrick et al., 2020; Lenderink et al., 2021). Wind shear affects MCS organisation (Moseley et al., 2016), the entrainment dilution of convection (Mulholland et al., 2021) and the inflow of unstable air and hence latent heating (Alfaro, 2017), thereby modifying MCS intensity (Mohr & Thorncroft, 2006). Environmental CAPE is another important driver for changes in MCS intensities and size (Prein et al., 2017; Maranan et al., 2018), but strongly co-varies with TCW and is therefore excluded from the driver scaling here to avoid double-counting. We therefore focus on future TCW and wind shear changes in CMIP models to reconstruct probable and time-continuous extreme MCS rainfall intensities.

Future changes in extreme rainfall and associated uncertainty are key parameters for defining long-term adaptation strategies against hydrological risks. The design of hydraulic infrastructures (e.g. sewage systems, dams) and their management relies on statistical indicators such as intensitiy-duration-frequency curves, design rainfall or floods, whose estimation in a changing climate remains a major challenge (François et al., 2019; Brunner et al., 2021; Sharma et al., 2021). This is particularly the case in West Africa, where hydraulic design tools are non-existent or obsolete (Sane et al., 2018). We illustrate a way to use CP models in combination with observations to inform the use of coarse-scale climate model data for such estimations. To our knowledge, this is the first attempt to combine this mixture of models and observations to better understand the response of future rainfall extremes to its atmospheric drivers.

2 Datasets and method

2.1 Observation-based data

Following the methodology in Klein et al. (2021), and drawing on previous West African studies (Arnaud et al., 1992; Laing et al., 1999; Mathon et al., 2002), we use thermal-

infrared imagery from the Meteosat series, which we combine with microwave rainfall estimates, and ERA5 reanalysis data over the West African monsoon season May-October 2004-2018 to relate MCS rainfall intensities to atmospheric drivers. Together, these datasets capture a broad range of MCS-driver variability under current climate conditions.

Based on 10.8 μm-band brightness temperatures of the Meteosat Second Generation (MSG, EUMETSAT, 2021; Schmetz et al., 2002), we identify MCSs as contiguous cloud $\leq$-50°C regions larger than 5000 km^2 between 16-1900UTC, the time when the frequency of MCSs reaches a maximum (e.g. Mathon & Laurent, 2001), for a Sahelian domain (9-19°N, 10W-15°E). Maximum MCS rainfall (P_{max}) is sampled from matched-up 'high-quality precipitation' (HQprecipitation, merged microwave-only precipitation estimate) fields of the half-hourly Final Run V06B Integrated Multi-satellitE Retrievals for Global Precipitation Measurement (IMERG-HQ; Huffman et al., 2019) dataset at ~15km resolution. MCS snapshots with $P_{max} \leq 1$ mm h^{-1} are removed to exclude non-precipitating cloud shields. We thus obtain conditional maximum rain rates from 22,368 MCS snapshots, for which we identify pre-storm driver conditions.

Environmental TCW and wind shear, defined here as the 925-600hPa zonal wind difference in m s^{-1}, are sampled from ERA5 reanalysis hourly data (Hersbach et al., 2020; CDS, 2021) coarsened to 0.7° resolution at 1200UTC, preceding afternoon MCSs, and at the location of minimum MCS temperature. The 0.7° resolution for atmospheric drivers reflects the scale of smallest considered MCSs while ensuring better consistency with the coarse spatial resolution of CMIP model data. For brevity, we refer to the combination of MSG, IMERG-HQ and ERA5 data for analyses as observation-based (OBS).

2.2 Convection-permitting model

This study uses data from the CP4 simulation; a 4.4km pan-African CP climate simulation based on the Met Office Unified Model and created within the Future Climate for Africa (FCFA) Improving Model Processes for African cLimAte (IMPALA) project (Stratton et al., 2018; Kendon et al., 2019). The modelled historical period ($CP4_H$) encompasses 1997-2006 with atmospheric boundary conditions provided by a prototype of the latest atmosphere-only UM global model GA7/GL7 at 25km with sea-surface temperatures (SST) prescribed from observations (Reynolds et al., 2007). The CP4 future projection ($CP4_F$) covers 10 years representative of 2100 climate conditions. It uses GA7/GL7

atmospheric boundary conditions under increased greenhouse gas concentrations in line with the Representative Concentration pathway (RCP) 8.5 at the end of this century. Driving SSTs are adjusted from $CP4_H$ to reflect end-of-century SSTs by adding a climatological annual cycle of ΔT derived from a HadGEM2-ES climate projection (Jones et al., 2011), while ozone and aerosol concentrations in $CP4_F$ remain the same as for $CP4_H$.

At ˜4.4km resolution, CP4 operates within the 'grey zone' for resolving convection (Field et al., 2017), but has been confirmed to improve the intensity and distribution of precipitation across the Sahel (Berthou, Rowell, et al., 2019). It also correctly captures climatological MCS distributions, albeit with underestimations in maximum MCS size and speeds together with an overestimation in MCS frequencies (Crook et al., 2019). We extract simulated afternoon MCSs following the same approach as for OBS, converting outgoing longwave radiation into brightness temperatures and applying the $\leq$-50°C temperature threshold. Filtering for $\geq$ 5000 km^2 rainy clouds gives 45,977 MCS snapshots for $CP4_H$ and 35,975 snapshots for $CP4_F$ with co-located atmospheric conditions sampled at 1200UTC and at 0.7° resolution. The smaller number of future MCSs is consistent with previous CP4 analyses, which found fewer but more intense rain events paired with longer dry spells across the Sahel for $CP4_F$ (Berthou, Kendon, et al., 2019; Kendon et al., 2019). In line with IMERG-HQ rainfall, the modelled rainfall is coarsened to 15km resolution before sampling MCS maximum rainfall. This averaging also reduces the overestimation of high-intensity rainfall CP4 shows at native resolution (cf. Fig. S1, Berthou, Rowell, et al., 2019).

2.3 CMIP models

We analyse driver changes in wind shear and TCW out to 2100 in simulations from 38 CMIP5 (Taylor et al., 2012) and 26 CMIP6 models (Eyring et al., 2016); one realisation per model i.e. 'r1i1p1' members (see supp. Table **??**) for which data were available for both variables. Only simulations forced by the RCP 8.5 (Shared Socioeconomic Pathway 5-8.5 for CMIP6) are analysed, consistent with CP4. Three different 30-year time slices are considered; 2030-2059 ("2040"), 2050-2079 ("2060"), and 2070-2099 ("2080"). The reference period covers 1950-1999, which was driven by historical anthropogenic and natural forcings. The models were interpolated onto a common 1.25° latitude x 1.875° longitude grid and averaged for respective time slices. For the rainfall reconstruction, we use a seasonal average of the changes in atmospheric drivers during the peak mon-

soon months July-September (JAS), during which MCS activity is at a maximum in the Sahel (Lafore et al., 2011; Nicholson, 2018). For a subset of models, we also evaluate changes in 3-hourly and daily rainfall extremes, depending on availability (c.f. supp. Table **??**).

2.4 Translating driver changes into changes in extreme rainfall

Using the identified MCSs from OBS and CP4, we define MCS extreme rainfall as the 95^{th} percentile of the maximum MCS rainfall distribution ($P_{max^{95}}$). We assume a linear relationship between changes in $\Delta P_{max^{95}}$ and atmospheric driver changes. The individual driver contribution is then defined as

$$\Delta P_{max^{95},t} = \beta_t \times \Delta TCW, \tag{1}$$

and

$$\Delta P_{max^{95},s} = \beta_s \times \Delta shear, \tag{2}$$

where ΔTCW and $\Delta shear$ denote the differences between JAS average future and historical conditions of the respective variable from either CMIP models or CP4. Reconstructed rainfall from JAS CP4-drivers will be used to evaluate our scaling approach in comparison to the CP4 *modelled* rainfall change. β_t and β_s represent the associated rainfall/driver relationships based on hourly atmospheric data, either as simulated by CP4 or derived from OBS. The change in driver-based $P_{max^{95}}$ is then reconstructed as a linear combination of individual driver contributions:

$$\Delta P_{max^{95},t+s} = \Delta P_{max^{95},t} + \Delta P_{max^{95},s}. \tag{3}$$

Our use of the driver scaling factors β_t and β_s depends on the precipitation/driver relationship remaining the same in the current and future climates, and on CP4 capturing the relationship under both climates. This will be discussed in the following.

3 Derived rainfall-driver relationships

3.1 Historical scaling of observed and modelled extreme rainfall with atmospheric drivers

We first evaluate how the rainfall-driver scaling compares between OBS and $CP4_H$ for the atmospheric drivers TCW and shear. In Fig. 1a,b, we stratify the MCS sample

according to driver strength and compute the 95^{th} percentile of the P_{max} distribution to obtain the intensity of the 5% most intense storms that can be supported by any joint TCW-shear combination (i.e. $P_{max^{95}}$). This allows us to ascertain how $P_{max^{95}}$ changes in response to one driver while the other remains approximately constant.

There is a marked tendency for $P_{max^{95}}$ to increase with higher TCW as well as with wind shear in OBS (Fig. 1a). This behaviour cannot be explained by any correlation between TCW and shear, which is negative for OBS (r=-0.21, p$\leq$0.01). $CP4_H$ similarly shows higher $P_{max^{95}}$ as TCW increases, but exhibits little sensitivity to ambient shear. Averaging across TCW-bins, Fig. 1c confirms that $CP4_H$ $P_{max^{95}}$-scaling with TCW shows good correspondence with a rainfall change of 0.69 mm h^{-1} per unit increase in TCW (mm) compared to 0.71 mm h^{-1} for OBS. At the same time, $CP4_H$ considerably underestimates the rainfall spread introduced by wind shear per TCW-bin (blue spread) and consequently does not reproduce the observed $P_{max^{95}}$-increase of 0.78 mm h^{-1} per unit shear (m s^{-1}) shown in Fig.1d.

This result is in line with previous studies of CP4, which found realistic MCS rainfall sensitivity to TCW but little shear dependency (Fitzpatrick et al., 2020; Senior et al., 2021). Our observation-based results however highlight the importance of shear for MCS maximum rainfall intensity on synoptic time scales; a relationship which is backed by theory (Alfaro, 2017) and can be captured by idealised models below 1km spatial resolution (Bickle et al., 2021).

We will therefore rely on the historical absolute $P_{max^{95}}$-shear scaling as inferred from OBS following Eq. 2 with β_s defined as

$$\beta_s = \left(\frac{\partial P_{max^{95}}}{\partial shear}\right)_{OBS} = 0.78 \pm 0.15 \ \frac{mm\ h^{-1}}{m\ s^{-1}} \ \ (\pm SE) \tag{4}$$

representing the absolute change in rainfall per unit shear from observations (Fig.1d) $\pm$ standard error SE. This is applied under the assumption that scaling of rainfall with wind shear remains constant across climates, which is supported by the good fit of the layer-lifting model of convection in Bickle et al. (2021), since this model depends on MCS-relative flows of moisture and hence shear. For TCW on the other hand, CP4 shows realistic behaviour, which we exploit in the next step to derive the scaling of $P_{max^{95}}$ with increasing TCW under global warming.

3.2 Future scaling of extreme rainfall with atmospheric moisture

Based on end-of-century projected changes by CP4, we now consider the climate change sensitivity of $P_{max^{95}}$ to TCW relative to the historical period. Different from the effect of wind shear, the rainfall-humidity relationship cannot be assumed to remain the same across climates as similar levels of TCW do not result in similar rainfall intensities.

This is illustrated in Fig. 2, where in addition to $CP4_H$, the pre-storm atmospheric drivers are separated for $CP4_F$ MCSs, similar to the approach used to obtain Fig. 1c, but by averaging the $P_{max^{95}}$ distribution across 5-percentile TCW-bins. Compared to $CP4_H$, the $CP4_F$ MCS distribution shows a marked shift towards higher TCW. At the same time, when MCSs occur, similar levels of TCW in $CP4_F$ result in higher $P_{max^{95}}$ than in $CP4_H$. This is in contrast to our current understanding for likely changes in *mean* rainfall, for which less rainfall is expected in a warmer climate for similar TCW, as more moisture is necessary to reach similar levels of relative humidity. A possible explanation for this behaviour is that extreme MCS rainfall occurs when convection is strong. Convective updraughts are expected to widen and intensify under global warming (Prein et al., 2017), with the latter similarly identified for CP4 (Jackson et al., 2020). The dynamical MCS intensification may then result in higher extreme rainfall in the future for similar TCW levels.

We follow a 'quantile-projection' approach to map the historical driver distribution and associated $P_{max^{95}}$ onto future conditions, as represented by climate change vectors β_t between $CP4_F$ and $CP4_H$ in Fig. 2. The resulting β_t ranges from 1.07 up to 1.33 (Fig. 2a inset), with a mean β_t according to

$$\beta_t = \overline{\left(\frac{\Delta P_{max^{95}}}{\Delta TCW}\right)}_{CP4} = 1.2 \pm 0.13\ h^{-1} \quad (\pm min/max) \tag{5}$$

The fact that hourly extreme rain scales with preceding TCW with $\beta_t > 1$ points towards the importance of dynamical processes that help to increase the vertical transport of moisture in MCSs and the MCS moisture supply from the surroundings. In the following, β_t is used to calculate $P_{max^{95},t}$ from TCW changes in CMIP models.

4 Combined driver-based projected changes in extreme rain

We now derive a plausible range of changes in reconstructed $\Delta P_{max^{95}}$ based on the Sahel domain-average of absolute changes in TCW (mm , Fig. 3a) and wind shear (m s^{-1}, Fig. 3b) of 64 CMIP models. The domain average is calculated for 9-19°N, 10W-15°E, in line with the domain where MCSs were sampled.

In terms of TCW and shear projections, there is no indication of a fundamentally different behaviour between CMIP5 and CMIP6 ensembles (Fig. 3a,b), justifying our pooled evaluation. For the 2080 period, the 10-90 percentile spread in TCW across all 64 CMIP models reaches +11-21 mm while CP4 projects a larger TCW change than 90% of all CMIP models (22 mm), noting it is representative of a later period and excludes anomalous aerosol forcing. Similarly, the CP4 wind shear change of +3 m s^{-1} is at the high end of the CMIP distribution.

Based on these results for ΔTCW and Δshear, we calculate $\Delta P_{max^{95},t}$, the rainfall contribution from TCW, via Eq. 1 using β_t as derived from CP4 (Eq. 5). The scaling factor β_s from OBS (Eq. 4) is directly applied in Eq. 2 to derive $\Delta P_{max^{95},s}$, the rainfall contribution from shear. By scaling the CMIP driver changes throughout the century, we can also obtain reconstructed $P_{max^{95}}$ intensities for the 2040 and 2060 periods, which are not covered by the CP4 simulation.

Using the combined information from OBS, CP4 and CMIP models, Figure 3c-e finally illustrates the translation of the MCS driver changes into absolute change in reconstructed $P_{max^{95}}$ for individual and combined drivers (c.f. Eq. 3) across the different future 30-year time slices:

$$\Delta P_{max^{95},t+s} = (\beta_t)_{CP4} \times (\Delta TCW)_{CMIP} + (\beta_s)_{OBS} \times (\Delta shear)_{CMIP}\,. \qquad (6)$$

Comparing TCW-reconstructed (Fig. 3c-e, grey line and shading) to the combined-driver $\Delta P_{max^{95}}$ (green line and shading), we find that shear changes have a minor effect on future rainfall change: while the individual change related to shear still increases from +1.8 mm h^{-1} around 2040 to +2.4 mm h^{-1} by 2080 for the 90^{th} CMIP percentile, the relative contribution from strengthened shear to total $\Delta P_{max^{95},t+s}$ decreases from 2040 through to 2100 as it is outpaced by the TCW increase. Hence, TCW remains the

primary driver of increased MCS extreme rainfall for all future time periods considering average driver changes across the Sahel.

4.1 Spatial variability of reconstructed extreme rainfall and comparison to modelled extremes

So far, presented results did not consider sub-regional driver variability. Across the Sahel domain, TCW changes show marked spatial variability linked to a pronounced zonal asymmetry in projected moisture changes as well as to generally strong meridional gradients in this wet-dry transition region (Figs. S2c, S3, S4). Strongest wind shear changes tend to follow zonal bands for CP4 and CMIP, for which most models suggest a peak in the eastern Sahel (Figs. S2d, S5, S6).

Assuming our domain-wide scaling factors remain valid locally, we calculate a pixel-based $\Delta P_{max^{95},t+s}$ for the 2080 period in Fig. 4a,b, showing the CMIP ensembles' 90th and 10th percentile, respectively. In line with model agreements on peaks of TCW and shear change in the eastern Sahel, the reconstructed $\Delta P_{max^{95},t+s}$ shows highest values over Niger and northern Nigeria. Shear contributions to $\Delta P_{max^{95},t+s}$ $\geq$8% up to a maximum of 17% (hatching) cover most of the northern Sahel for both extreme ends of the CMIP range, commensurate with large CMIP uncertainties in modelling changes in southern Saharan lower tropospheric warming (Rowell et al., 2021).

Finally, we compare relative changes in reconstructed $\Delta P_{max^{95}t+s}$ with modelled rainfall changes in CP4 and CMIP (Fig. 4c). The scaling is compared for the Sahel domain and boxes centred on the cities of Bamako (1), Timbuktu (2), and Niamey (3) (Fig. 4a), corresponding to regions along the previously discussed zonal gradient of TCW change projected by many CMIP models. For CP4, this step provides an indication of the skill of the simple linear driver-scaling presented here to reproduce regional intensities of modelled MCS rainfall. Figure 4c illustrates that for all regions except Bamako, the CP4-modelled $\Delta P_{max^{95}}$ (black cross) lies within the uncertainty range of $\Delta P_{max^{95}t+s}$ reconstructed from JAS CP4 driver changes (green cross and shading). The range reflects the uncertainty associated with the TCW and shear scaling factors and reaches a maximum of $\pm$7.7% (Niamey). This good correspondence in spite of CP4's weak shear response may be linked to the scaling not considering additional rainfall intensification factors like instability, suggesting that our results may still be a conservative estimate.

The CMIP5/6-based $\Delta P_{max^{95}t+s}$ (green box) is shown in comparison to the modelled change in 95^{th} percentile daily rainfall (for wet days $\geq$0.1mm) of a range of raw CMIP5/6 models (grey box) as well as to a bias-corrected version of CMIP5 (blue box). We consider the latter to be the best available dataset regarding CMIP5-projected rainfall changes in West Africa (Famien et al., 2018). Across evaluated regions, the ensemble mean change in reconstructed extreme rainfall lies between +40-58% (+20-31% for the 2040 period), which is markedly higher than for any ensemble-mean modelled CMIP rainfall in the same region. Furthermore, $\Delta P_{max^{95}t+s}$ shows a clear signal of intensification across the entire CMIP uncertainty range, linked to exclusively positive driver changes. Modelled daily extremes on the other hand include negative changes within the 10-90^{th} percentile CMIP range for all regions, with region-dependent ensemble means between 14-35% for raw CMIP and 3-48% for bias-corrected CMIP5. While we acknowledge that the change in $\Delta P_{max^{95}t+s}$, which is based on sub-daily extremes, may behave differently from CMIP daily rainfall metrics, it allows us to compare the reconstructed results to a more commonly-used and directly-inferred extreme rainfall metric. In addition, 3 out of 4 currently available CMIP6 models that provide sub-daily rainfall did not show a stronger signal for 3-hourly compared to daily extremes (Fig. S7), suggesting there is no systematic intensification at sub-daily scale that applies to all CMIP models.

5 Discussion and conclusions

In this study, our aim was to fuse a CP model projection, which provides us with only one possible future of how precipitation extremes from West African MCSs might change, with a CMIP-based time-continuous uncertainty range. For that, we adopted a simple linear scaling based on only TCW and shear, which we show allows to reconstruct CP4-modelled rainfall intensities. The presented scaling approach follows the assumption that CMIP changes in atmospheric drivers of MCSs are plausible, while the CP model in combination with observations provides a more realistic response of extreme MCS rainfall to those drivers. We thus draw on the strengths of respective datasets.

We find reconstructed changes in extreme rainfall to be exclusively positive across CMIP models, dominated by the strong projected increases in TCW with an ensemble 10-90 percentile range of +37-75% (+55% mean) for 2070-2100 (+18-30% with +26% mean for 2030-2060) under RCP8.5 across our Sahel domain. Shear contributions to these figures reach at least 8% for most of the northern Sahel, although we note that this re-

sult is based on MCS sensitivities to shear in the afternoon. The shear contribution may be higher for nocturnal MCSs, when the importance of shear for MCS maintenance increases in the absence of daytime heating (e.g. Vizy & Cook, 2018). The strictly positive changes are in contrast to CMIP-modelled changes in daily extremes, which we find to be less conclusive with a 10-90 percentile range of +0-60% (+30% mean) for raw CMIP5/6 rainfall and +4-88% (+37% mean) using a bias-corrected CMIP5 dataset with some models again exhibiting negative changes.

The limited previous analyses of extreme rainfall projections over West Africa to date focus on selections of RCP8.5 downscaled CMIP models and have found either little change in extreme precipitation trends compared to driving CMIP models with no agreement in sign (Diallo et al., 2016) or end-of-century ensemble-mean increases that stay below 40% (Sylla et al., 2015; Todzo et al., 2020). This suggests, CMIP and even medium-resolution downscaling approaches may consistently underestimate extreme rainfall change, potentially in ways related to model resolution, convection schemes and projected driver changes. This conclusion is further supported by previous CP4 studies (Kendon et al., 2019; Finney et al., 2020; Jackson et al., 2020).

While the driver-reconstructed change in extreme rainfall presented here exhibits an apparently smaller uncertainty range than that of the CMIP models, many assumptions and simplifications are incorporated in the reconstruction that are not explicitly reflected. For example, we assume that the driver changes MCSs feel locally on an hourly basis are proportional to the climate change in the July-September domain mean as represented in the CMIP driver data. We also necessarily assume that rainfall scaling with wind shear is stationary across climates since the CP model fails to capture the observed shear sensitivity, highlighting a key problem of this CP simulation - although related errors would be minor given the indicated secondary role of wind shear for future extreme rain intensification. Furthermore, various scaling problems are simplified by the fact that all changes in the considered drivers are positive and force extreme rain in the same direction with climate change, avoiding drivers cancelling each other, which would considerably increase the significance of scaling errors. We also use the historical CP4 rainfall distribution as a present-day reference to translate the reconstructed absolute rainfall changes into relative changes, even though certain CMIP future driver changes may be unlikely given the CP4 historical starting point. Nevertheless, for simplicity, we assume all CMIP driver changes to be equally plausible to occur in CP4.

This leaves us with a novel methodology that combines CP with CMIP simulations and observations to translate future atmospheric changes into extreme rainfall change. The reconstructed extreme rainfall illustrates that, given the background conditions for MCS formation in a region, associated rainfall extremes will increase in line with and beyond the regional increase in TCW if relative humidity remains approximately constant. This relationship, diagnosed from CP simulations, makes TCW change a useful indicator for the behaviour of the extreme tail of the rainfall distribution. In this way, an evaluation of convection-permitting rainfall projections based on atmospheric drivers helps to communicate to users more defensible hydro-climatological information for West Africa, using our best scientific knowledge and understanding of the likely future changes in MCSs. The logical framing of this approach also lends itself to the construction of climate-change narratives (e.g. Dessai et al., 2018; Burgin et al., 2020), which have been found to be very useful in risk communication.

Acknowledgments

The research leading to these results received funding from the U.K.'s Natural Environment Research Council/Department for International Development (NERC/DFID) Future Climate for Africa (FCFA) program, under the AMMA-2050 (grant numbers NE/M020126/1, NE/M019977/1, NE/M019969/1, NE/M019950/1, NE/M019934/1, NE/M020428/2, NE/M020428/1) and Improving Model Processes for African Climate (IMPALA) projects (NE/MO17176/1, NE/M017230/1). Marsham also acknowledges funding from the HyCRISTAL project (NE/M02038X/1). We thank Rachel Stratton and Simon Vosper (Met Office), who ran the CP4 simulations within IMPALA and made the data available. Instructions for access to the CP4 dataset can be found in the User Guide via https://futureclimateafrica.org/wp-content/uploads/2020/12/FCFA-CP4A-full-guide-final.pdf and are publicly available from the Centre for Environmental Data Analysis (CEDA) archive (http://archive.ceda.ac.uk/). MSG data are available from the EUMETSAT archive https://navigator.eumetsat.int /product/EO:EUM:DAT:MSG:HRSEVIRI, ECMWF hourly ERA5 reanalysis data are available from the Copernicus Data Store (https://doi.org/10.24381/cd and data from the Global Precipitation Measurement mission are available from https://doi.org/10.5067/GPM/IM HH/06. We also acknowledge the World Climate Research Programme, which, through its Working Group on Coupled Modelling, coordinated and promoted CMIP. We thank the climate modeling groups for producing and making available their model output, the Earth System Grid Federation (ESGF) for archiving the data and providing access, and

the multiple funding agencies who support CMIP5 (https://esgf-node.llnl.gov/projects/cmip5/), CMIP6 and ESGF, and we thank the involved climate modeling groups for producing and making available their model output. Special thanks go to the developers of the Pangeo CMIP6 data access and cloud processing (https://pangeo-data.github.io/pangeo-cmip6-cloud/accessing_data.html), which worked like a charm, and to the providers of the python packages matplotlib/cartopy, xarray, salem, scipy, metpy, pandas, and their dependencies.

6 Data availability statement

The data that support the findings of this study are openly available except for the bias-corrected CMIP5 dataset, which can be obtained by contacting AD: moise.famien@locean.ipsl.fr

7 Author contribution

CK, LJ, DP, JM, CT, DR and FG conceptualised the study, with input from TV and AD. All authors contributed to and discussed the methodological design, and analyses were conducted by CK and LJ, with input from AF. CK and DP led the writing of the manuscript, with contributions from all authors.

References

Alfaro, D. A. (2017, jan). Low-tropospheric shear in the structure of squall lines: Impacts on latent heating under layer-lifting ascent. *Journal of the Atmospheric Sciences*, *74*(1), 229–248. doi: 10.1175/JAS-D-16-0168.1

Allen, M. R., & Ingram, W. J. (2002). Constraints on future changes in climate and the hydrologic cycle. *Nature*, *419*(6903). doi: 10.1038/nature01092

Arnaud, Y., Desbois, M., & Maizi, J. (1992, may). Automatic tracking and characterization of African convective systems on Meteosat pictures. *Journal of Applied Meteorology*, *31*(5), 443–453. doi: 10.1175/1520-0450(1992)031⟨0443:ATACOA⟩2.0.CO;2

Berthou, S., Kendon, E. J., Rowell, D. P., Roberts, M. J., Tucker, S., & Stratton, R. A. (2019, nov). Larger Future Intensification of Rainfall in the West African Sahel in a Convection-Permitting Model. *Geophysical Research Letters*, *46*(22), 13299–13307. doi: 10.1029/2019GL083544

Berthou, S., Rowell, D. P., Kendon, E. J., Roberts, M. J., Stratton, R. A., Crook,

J. A., & Wilcox, C. (2019, aug). Improved climatological precipitation characteristics over West Africa at convection-permitting scales. *Climate Dynamics*, *53*(3-4), 1991–2011. Retrieved from https://doi.org/10.1007/s00382-019-04759-4http://link.springer.com/10.1007/s00382-019-04759-4 doi: 10.1007/s00382-019-04759-4

Bickle, M. E., Marsham, J. H., Ross, A. N., Rowell, D. P., Parker, D. J., & Taylor, C. M. (2021, jan). Understanding mechanisms for trends in Sahelian squall lines: Roles of thermodynamics and shear. *Quarterly Journal of the Royal Meteorological Society*, *147*(735), 983–1006. doi: 10.1002/qj.3955

Brunner, M. I., Slater, L., Tallaksen, L. M., & Clark, M. (2021, may). Challenges in modeling and predicting floods and droughts: A review. *WIREs Water*, *8*(3), e1520. doi: 10.1002/wat2.1520

Burgin, L., Rowell, D. P., & Marsham, J. H. (2020). Possible futures for East Africa under a changing climate: Technical appendix for HyCRISTAL's Climate Risk Narratives.
doi: http://doi.org/10.5281/zenodo.3620757

CDS. (2021). *Copernicus Climate Data Store: ERA, Fifth generation of ECMWF atmospheric reanalyses of the global climate.* Retrieved 2020-01-14, from https://cds.climate.copernicus.eu/cdsapp#!/dataset/reanalysis-era5-pressure-levels?tab=overview doi: 10.24381/cds.bd0915c6

Coppola, E., Sobolowski, S., Pichelli, E., Raffaele, F., Ahrens, B., Anders, I., ... Warrach-Sagi, K. (2020). *A first-of-its-kind multi-model convection permitting ensemble for investigating convective phenomena over Europe and the Mediterranean* (Vol. 55) (No. 1-2). doi: 10.1007/s00382-018-4521-8

Crook, J., Klein, C., Folwell, S., Taylor, C. M., Parker, D. J., Stratton, R., & Stein, T. (2019, may). Assessment of the Representation of West African Storm Lifecycles in Convection-Permitting Simulations. *Earth and Space Science*, *6*(5), 818–835. doi: 10.1029/2018EA000491

Dessai, S., Bhave, A., Birch, C., Conway, D., Garcia-Carreras, L., Gosling, J. P., ... Stainforth, D. (2018). Building narratives to characterise uncertainty in regional climate change through expert elicitation. *Environmental Research Letters*, *13*(7). doi: 10.1088/1748-9326/aabcdd

Diallo, I., Giorgi, F., Deme, A., Tall, M., Mariotti, L., & Gaye, A. T. (2016, dec). Projected changes of summer monsoon extremes and hydroclimatic regimes over West Africa for the twenty-first century. *Climate Dynamics*, *47*(12), 3931–3954. Retrieved from `http://link.springer.com/10.1007/s00382-016-3052-4` doi: 10.1007/s00382-016-3052-4

Engel, T., Fink, A. H., Knippertz, P., Pante, G., & Bliefernicht, J. (2017, nov). Extreme precipitation in the West African cities of Dakar and Ouagadougou: Atmospheric dynamics and implications for flood risk assessments. *Journal of Hydrometeorology*, *18*(11), 2937–2957. doi: 10.1175/JHM-D-16-0218.1

EUMETSAT. (2021). *High Rate SEVIRI Level 1.5 Image Data - MSG - 0 degree.* Retrieved 2021-08-25, from `https://navigator.eumetsat.int/product/EO:EUM:DAT:MSG:HRSEVIRI`

Eyring, V., Bony, S., Meehl, G. A., Senior, C. A., Stevens, B., Stouffer, R. J., & Taylor, K. E. (2016). Overview of the Coupled Model Intercomparison Project Phase 6 (CMIP6) experimental design and organization. *Geoscientific Model Development*, *9*(5), 1937–1958. doi: 10.5194/gmd-9-1937-2016

Famien, A. M., Janicot, S., Delfin Ochou, A., Vrac, M., Defrance, D., Sultan, B., & Noël, T. (2018). A bias-corrected CMIP5 dataset for Africa using the CDF-t method - A contribution to agricultural impact studies. *Earth System Dynamics*, *9*(1), 313–338. doi: 10.5194/esd-9-313-2018

Field, P. R., Brozková, R., Chen, M., Dudhia, J., Lac, C., Hara, T., ... McTaggart-Cowan, R. (2017). Exploring the convective grey zone with regional simulations of a cold air outbreak. *Quarterly Journal of the Royal Meteorological Society*, *143*(707), 2537–2555. doi: 10.1002/qj.3105

Finney, D. L., Marsham, J. H., Rowell, D. P., Kendon, E. J., Tucker, S. O., Stratton, R. A., & Jackson, L. S. (2020, apr). Effects of explicit convection on future projections of mesoscale circulations, rainfall, and rainfall extremes over eastern Africa. *Journal of Climate*, *33*(7), 2701–2718. doi: 10.1175/JCLI-D-19-0328.1

Fitzpatrick, R. G., Parker, D. J., Marsham, J. H., Rowell, D. P., Guichard, F. M., Taylor, C. M., ... Tucker, S. (2020). What drives the intensification of mesoscale convective systems over the West African Sahel under climate change? *Journal of Climate*, *33*(8), 3151–3172. doi: 10.1175/

JCLI-D-19-0380.1

Fosser, G., Kendon, E. J., Stephenson, D., & Tucker, S. (2020, jul). Convection-Permitting Models Offer Promise of More Certain Extreme Rainfall Projections. *Geophysical Research Letters*, *47*(13), 0–2. doi: 10.1029/2020GL088151

François, B., Schlef, K., Wi, S., & Brown, C. (2019, jul). Design considerations for riverine floods in a changing climate – A review. *Journal of Hydrology*, *574*, 557–573. doi: 10.1016/j.jhydrol.2019.04.068

Hersbach, H., Bell, B., Berrisford, P., Hirahara, S., Horányi, A., Muñoz-Sabater, J., ... Thépaut, J. N. (2020, jul). The ERA5 global reanalysis. *Quarterly Journal of the Royal Meteorological Society*, *146*(730), 1999–2049. doi: 10.1002/qj.3803

Huffman, G., Stocker, E., Bolvin, D., Nelkin, E., & Tan, J. (2019). *GPM IMERG Final Precipitation L3 Half Hourly 0.1 degree x 0.1 degree V06, Greenbelt, MD, Goddard Earth Sciences Data and Information Services Center (GES DISC)* (Vol. 01) (No. 02). Retrieved 25/08/2021, from `https://disc.gsfc.nasa.gov/datasets/GPM_3IMERGHH_06/summary` doi: 10.5067/GPM/IMERG/3B-HH/06

IPCC Working Group 1, I., Stocker, T., Qin, D., Plattner, G.-K., Tignor, M., Allen, S., ... Midgley, P. (2013). *IPCC, 2013: Climate Change 2013: The Physical Science Basis. Contribution of Working Group I to the Fifth Assessment Report of the Intergovernmental Panel on Climate Change* (Vol. AR5). Cambridge University Press, Cambridge, United Kingdom and New York, NY, USA.

Jackson, L. S., Finney, D. L., Kendon, E. J., Marsham, J. H., Parker, D. J., Stratton, R. A., ... Tucker, S. (2020, oct). The effect of explicit convection on couplings between rainfall, humidity, and ascent over Africa under climate change. *Journal of Climate*, *33*(19), 8315–8337. doi: 10.1175/JCLI-D-19-0322.1

Jones, C. D., Hughes, J. K., Bellouin, N., Hardiman, S. C., Jones, G. S., Knight, J., ... Zerroukat, M. (2011). The HadGEM2-ES implementation of CMIP5 centennial simulations. *Geoscientific Model Development*, *4*(3), 543–570. doi: 10.5194/gmd-4-543-2011

Kendon, E. J., Ban, N., Roberts, N. M., Fowler, H. J., Roberts, M. J., Chan, S. C., ... Wilkinson, J. M. (2017). Do convection-permitting regional climate models

improve projections of future precipitation change? *Bulletin of the American Meteorological Society*, *98*(1), 79–93. doi: 10.1175/BAMS-D-15-0004.1

Kendon, E. J., Stratton, R. A., Tucker, S., Marsham, J. H., Berthou, S., Rowell, D. P., & Senior, C. A. (2019). Enhanced future changes in wet and dry extremes over Africa at convection-permitting scale. *Nature Communications*, *10*(1). doi: 10.1038/s41467-019-09776-9

Klein, C., Nkrumah, F., Taylor, C. M., & Adefisan, E. A. (2021). Seasonality and trends of drivers of mesoscale convective systems in Southern West Africa. *Journal of Climate*, *34*(1), 71–87. doi: 10.1175/JCLI-D-20-0194.1

Lafore, J. P., Flamant, C., Guichard, F., Parker, D. J., Bouniol, D., Fink, A. H., ... Thorncroft, C. (2011). Progress in understanding of weather systems in West Africa. *Atmospheric Science Letters*, *12*(1), 7–12. doi: 10.1002/asl.335

Laing, A. G., Fritsch, J. M., & Negri, A. J. (1999). Contribution of mesoscale convective complexes to rainfall in Sahelian Africa: Estimates from geostationary infrared and passive microwave data. *Journal of Applied Meteorology*, *38*(7), 957–964. doi: 10.1175/1520-0450(1999)038⟨0957:COMCCT⟩2.0.CO;2

Lavin-Gullon, A., Feijoo, M., Solman, S., Fernandez, J., da Rocha, R. P., & Bettolli, M. L. (2021). Synoptic forcing associated with extreme precipitation events over Southeastern South America as depicted by a CORDEX FPS set of convection-permitting RCMs. *Climate Dynamics*, *56*(9-10), 3187–3203. doi: 10.1007/s00382-021-05637-8

Lenderink, G., De Vries, H., Fowler, H. J., Barbero, R., Van Ulft, B., & Van Meijgaard, E. (2021, apr). Scaling and responses of extreme hourly precipitation in three climate experiments with a convection-permitting model. *Philosophical Transactions of the Royal Society A: Mathematical, Physical and Engineering Sciences*, *379*(2195), 20190544. doi: 10.1098/rsta.2019.0544

Lobell, D. B., & Gourdji, S. M. (2012). The influence of climate change on global crop productivity. *Plant Physiology*, *160*(4), 1686–1697. doi: 10.1104/pp.112.208298

Maranan, M., Fink, A. H., & Knippertz, P. (2018, jul). Rainfall types over southern West Africa: Objective identification, climatology and synoptic environment. *Quarterly Journal of the Royal Meteorological Society*, *144*(714), 1628–1648. doi: 10.1002/qj.3345

Mathon, V., & Laurent, H. (2001). Life cycle of Sahelian mesoscale convective cloud systems. *Quarterly Journal of the Royal Meteorological Society*, *127*, 377–406.

Mathon, V., Laurent, H., & Lebel, T. (2002, nov). Mesoscale convective system rainfall in the Sahel. *Journal of Applied Meteorology*, *41*(11), 1081–1092. doi: 10.1175/1520-0450(2002)041⟨1081:MCSRIT⟩2.0.CO;2

Mohr, K. I., & Thorncroft, C. D. (2006, jan). Intense convective systems in West Africa and their relationship to the African easterly jet. *Quarterly Journal of the Royal Meteorological Society*, *132*(614), 163–176. doi: 10.1256/qj.05.55

Moseley, C., Hohenegger, C., Berg, P., & Haerter, J. O. (2016). Intensification of convective extremes driven by cloud-cloud interaction. *Nature Geoscience*, *9*(10), 748–752. doi: 10.1038/ngeo2789

Mulholland, J. P., Peters, J. M., & Morrison, H. (2021, apr). How does vertical wind shear influence entrainment in squall lines? *Journal of the Atmospheric Sciences*, *78*(6), 1931–1946. doi: 10.1175/jas-d-20-0299.1

Nicholson, S. E. (2018). *Climate of the Sahel and West Africa* (Vol. 510) (No. July). doi: 10.1093/acrefore/9780190228620.013.510

O'Gorman, P. A., & Schneider, T. (2009, sep). The physical basis for increases in precipitation extremes in simulations of 21st-century climate change. *Proceedings of the National Academy of Sciences of the United States of America*, *106*(35), 14773–14777. Retrieved from `http://www.pnas.org/cgi/doi/10.1073/pnas.0907610106` doi: 10.1073/pnas.0907610106

Prein, A. F., Langhans, W., Fosser, G., Ferrone, A., Ban, N., Goergen, K., ... Leung, R. (2015, jun). A review on regional convection-permitting climate modeling: Demonstrations, prospects, and challenges. *Reviews of Geophysics*, *53*(2), 323–361. doi: 10.1002/2014RG000475

Prein, A. F., Liu, C., Ikeda, K., Trier, S. B., Rasmussen, R. M., Holland, G. J., & Clark, M. P. (2017). Increased rainfall volume from future convective storms in the US. *Nature Climate Change*, *7*(12), 880–884. Retrieved from `http://dx.doi.org/10.1038/s41558-017-0007-7` doi: 10.1038/s41558-017-0007-7

Reynolds, R. W., Smith, T. M., Liu, C., Chelton, D. B., Casey, K. S., & Schlax, M. G. (2007). Daily high-resolution-blended analyses for sea surface temperature. *Journal of Climate*, *20*(22), 5473–5496. doi: 10.1175/2007JCLI1824.1

Roderick, T. P., Wasko, C., & Sharma, A. (2019). Atmospheric Moisture Measurements Explain Increases in Tropical Rainfall Extremes. *Geophysical Research Letters*, *46*(3), 1375–1382. doi: 10.1029/2018GL080833

Rowell, D. P., Fitzpatrick, R. G., Jackson, L. S., & Redmond, G. (2021). Understanding intermodel variability in future projections of a sahelian storm proxy and southern saharan warming. *Journal of Climate*, *34*(2), 509–525. doi: 10.1175/JCLI-D-20-0382.1

Sane, Y., Panthou, G., Bodian, A., Vischel, T., Lebel, T., Dacosta, H., ... Diop Kane, M. (2018). Intensity-duration-frequency (IDF) rainfall curves in Senegal. *Natural Hazards and Earth System Sciences*, *18*(7), 1849–1866. doi: 10.5194/nhess-18-1849-2018

Schmetz, J., Pili, P., Tjemkes, S., Just, D., Kerkmann, J., Rota, S., & Ratier, A. (2002, jul). An Introduction to Meteosat Second Generation (MSG). *Bulletin of the American Meteorological Society*, *83*(7), 977–992. Retrieved from `http://www.eumetsat.inthttps://journals.ametsoc.org/view/journals/bams/83/7/1520-0477_2002_083_0977_aitmsg_2_3_co_2.xml` doi: 10.1175/1520-0477(2002)083⟨0977:AITMSG⟩2.3.CO;2

Senior, C. A., Marsham, J. H., Berthou, S., Burgin, L. E., Folwell, S. S., Kendon, E. J., ... Willet, M. R. (2021, feb). Convection permitting regional climate change simulations for understanding future climate and informing decision making in Africa. *Bulletin of the American Meteorological Society*, 1–46. doi: 10.1175/bams-d-20-0020.1

Sharma, A., Hettiarachchi, S., & Wasko, C. (2021, apr). Estimating design hydrologic extremes in a warming climate: Alternatives, uncertainties and the way forward. *Philosophical Transactions of the Royal Society A: Mathematical, Physical and Engineering Sciences*, *379*(2195), 20190623. doi: 10.1098/rsta.2019.0623

Stephens, G. L., L'Ecuyer, T., Forbes, R., Gettlemen, A., Golaz, J. C., Bodas-Salcedo, A., ... Haynes, J. (2010). Dreary state of precipitation in global models. *Journal of Geophysical Research Atmospheres*, *115*(24), 1–14. doi: 10.1029/2010JD014532

Stratton, R. A., Senior, C. A., Vosper, S. B., Folwell, S. S., Boutle, I. A., Earnshaw, P. D., ... Wilkinson, J. M. (2018, may). A Pan-African convection-permitting

regional climate simulation with the met office unified model: CP4-Africa. *Journal of Climate*, *31*(9), 3485–3508. doi: 10.1175/JCLI-D-17-0503.1

Sylla, M. B., Giorgi, F., Pal, J. S., Gibba, P., Kebe, I., & Nikiema, M. (2015). Projected changes in the annual cycle of high-intensity precipitation events over West Africa for the late twenty-first century. *Journal of Climate*, *28*(16), 6475–6488. doi: 10.1175/JCLI-D-14-00854.1

Taylor, K. E., Stouffer, R. J., & Meehl, G. A. (2012). An overview of CMIP5 and the experiment design. *Bulletin of the American Meteorological Society*, *93*(4), 485–498. doi: 10.1175/BAMS-D-11-00094.1

Todzo, S., Bichet, A., & Diedhiou, A. (2020). Intensification of the hydrological cycle expected in West Africa over the 21st century. *Earth System Dynamics*, *11*(1), 319–328. doi: 10.5194/esd-11-319-2020

Trenberth, K. E., Dai, A., Rasmussen, R. M., & Parsons, D. B. (2003). The changing character of precipitation. *Bulletin of the American Meteorological Society*, *84*(9), 1205–1217+1161. doi: 10.1175/BAMS-84-9-1205

Vischel, T., & Lebel, T. (2007, feb). Assessing the water balance in the Sahel: Impact of small scale rainfall variability on runoff. Part 2: Idealized modeling of runoff sensitivity. *Journal of Hydrology*, *333*(2-4), 340–355. doi: 10.1016/j.jhydrol.2006.09.007

Vizy, E. K., & Cook, K. H. (2018). Mesoscale convective systems and nocturnal rainfall over the West African Sahel: role of the Inter-tropical front. *Climate Dynamics*, *50*(1-2), 587–614. doi: 10.1007/s00382-017-3628-7

Zhou, X., Yang, K., Ouyang, L., Wang, Y., Jiang, Y., Li, X., ... Prein, A. (2021). Added value of kilometer-scale modeling over the third pole region: a CORDEX-CPTP pilot study. *Climate Dynamics*(0123456789). doi: 10.1007/s00382-021-05653-8

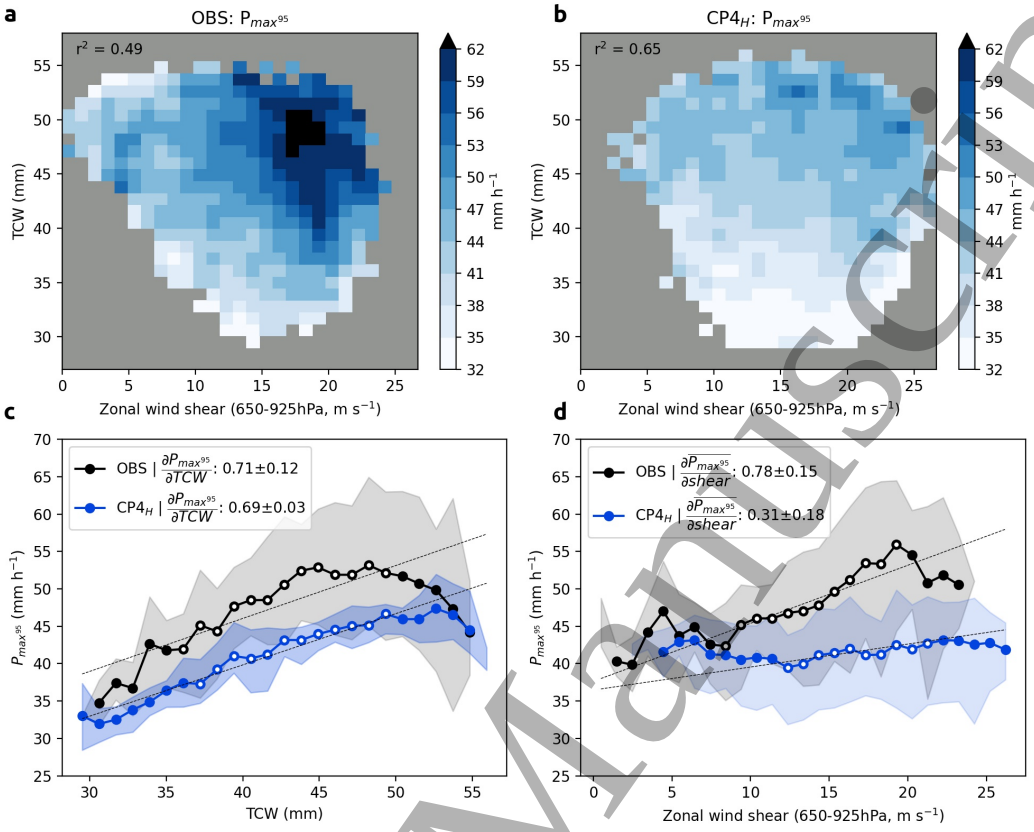

Figure 1. Comparison of extreme rainfall-driver scaling in observations and CP simulation. 2D-histograms of $P_{max^{95}}$ intensity for pre-storm TCW (mm) versus zonal wind shear (m s^{-1}) for (a) OBS (ERA5, IMERG) and (b) $CP4_H$. Bins with fewer than 10 MCSs are shaded grey. r^2 gives explained $P_{max^{95}}$ variance from multi-linear regression of TCW and shear. Line plots are based on the histograms, depicting the $P_{max^{95}}$ relationship with (c) TCW only (d) shear only, for OBS (black) and $CP4_H$ (blue). Shading spans the 10-90 percentile spread of (c) shear-related $P_{max^{95}}$ across each TCW bin, and of (d) TCW-related $P_{max^{95}}$ across each shear bin. Legends give slopes of the linear fits (black dashed lines, p≤0.01 except $CP4_H$ shear fit) ± standard errors), weighted by MCS number per joint driver bin. Empty circles indicate bins cumulatively containing 80% of all MCSs.

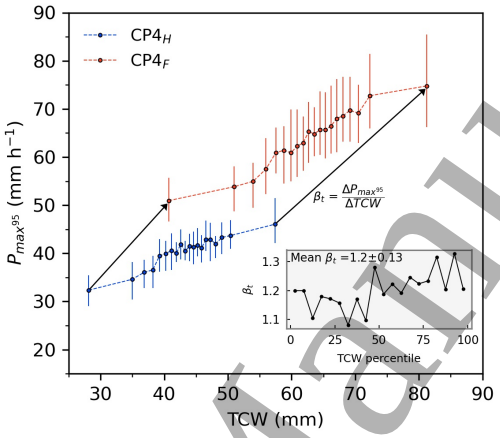

Figure 2. Deriving extreme MCS precipitation scaling from projected moisture change in the CP simulation. $P_{max^{95}}$ (mm h^{-1}) for 5-%tile bins as a function of pre-storm TCW (mm) for CP4-historical (CP4$_H$, blue) and -future (CP4$_F$, red) with bars spanning the 10-90 percentile of shear bins as in Fig. 1. The scaling factor (inset) is calculated for each percentile-connecting vector (β_t, two example vectors given), expressed as the absolute change of $P_{max^{95}}$ per change in TCW between CP4$_H$ and CP4$_F$.

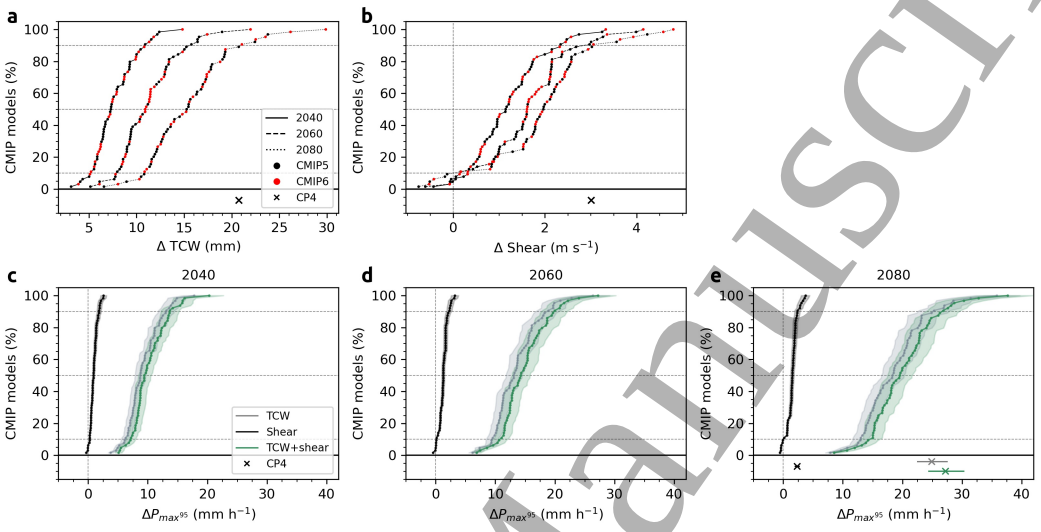

Figure 3. CMIP driver change and reconstructed extreme rainfall from combined drivers. Sahel domain-average driver change of value-ordered CMIP5 (n=38) and CMIP6 (n=26) models for (a) TCW (mm) and (b) wind shear (m s^{-1}) for the 2040, 2060, and 2080 periods relative to historical. CP4 driver change is based on JAS domain-averages, in line with CMIP, and corresponds to circa 2100. (c,d,e) shows the driver-reconstructed change in $P_{max^{95}}$ (mm h^{-1}) for respective time periods associated with TCW (grey), zonal wind shear (black), and combined change (green) for all models. Shading for CMIP and whiskers for CP4 depict uncertainty range from scaling with β_s=0.78±0.15 and β_t=1.2±0.13.

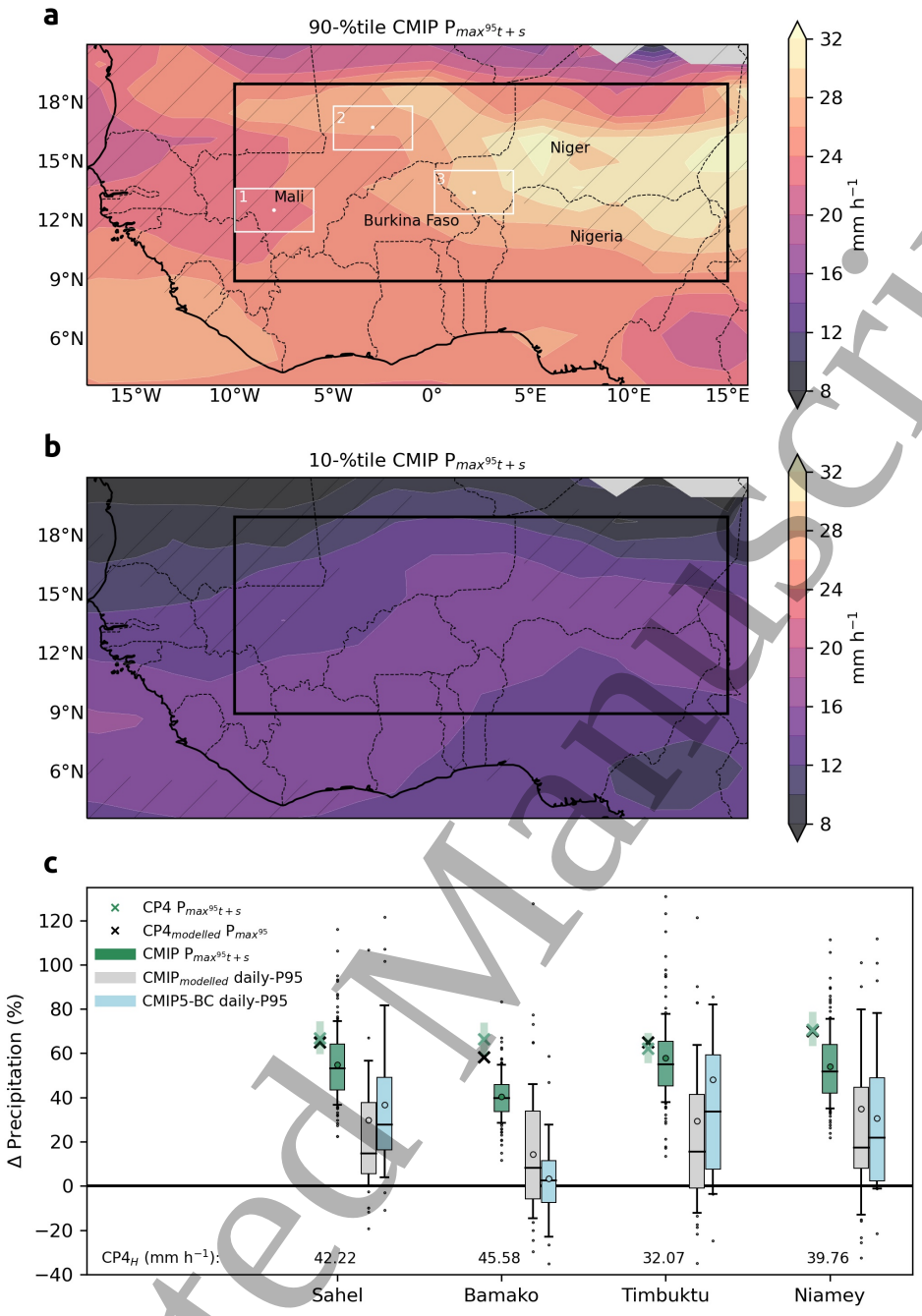

Figure 4. Spatial reconstruction of extreme rainfall change and comparison to modelled change for 2080. (a,b) shows driver-reconstructed $\Delta\ P_{max^{95},t+s}$ (mm h^{-1}) for the 90th and 10th percentiles across the CMIP ensemble (n=64) at each grid point, respectively, and areas of wind shear contribution ≥8% to the rainfall change (hatching). Large box marks the Sahel domain for which β_t and β_s were derived and 2°x1° boxes are centred on the cities of Bamako (1), Niamey (2), and Timbuktu (3). (c) compares relative changes in $\Delta\ P_{max^{95},t+s}$ based on CMIP driver change (green boxes) to CMIP-modelled 95^{th} percentile daily rainfall (grey boxes, n=47) and for a bias-corrected CMIP5 version ((Famien et al., 2018), blue boxes, n=28). Boxplots span the inter-quartile range, indicating the median (line) and mean (open circles), with 10-90 percentile whiskers. (x) depict CP4 driver-reconstructed $\Delta P_{max^{95},t+s}$ (green x), and the raw CP4-modelled rainfall (black x). Green shading for CP4-(x) depicts the uncertainty from β_t and β_s scaling factors.